Neuromuscular Strategies during Cycling at Different Muscular Demands

HENDRIK ENDERS, VINZENZ VON TSCHARNER, and BENNO M. NIGG

Human Performance Laboratory, Faculty of Kinesiology, University of Calgary, Calgary, AB, CANADA

ABSTRACT

ENDERS, H., V. VON TSCHARNER, and B. M. NIGG. Neuromuscular Strategies during Cycling at Different Muscular Demands. *Med. Sci. Sports Exerc.*, Vol. 47, No. 7, pp. 1450–1459, 2015. **Purpose**: This study investigated muscle coordination while pedaling at 150 and 300 W with a cadence of 90 rpm. Changes in the variability of the electromyographic (EMG) signals were quantified in 14 subjects. **Methods**: Principal component analysis was used to find correlated EMG patterns among seven leg muscles that reflect neuromuscular strategies while pedaling. Sample entropy was used to assess the regularity of the short-term fluctuations of the EMG. Signal structure relates to the autocorrelation and to the information in the phase of the signal. This study used the information encrypted in the phase to quantify neuromuscular control and compared the results to phase-randomized surrogate data. **Results**: Although the pattern remained similar, the correlation between individual muscles showed effort-dependent differences. Increased workload altered the overall neuromuscular strategy indicated by changes in the contribution of individual muscles to the movement. Additionally, the executed strategy was characterized by increased structure. Regularity of the short-term fluctuations in the EMG increased significantly with effort level. Both experimental conditions showed more structure in the phase of the EMG compared to the surrogate data. **Conclusions**: This increased structure in the EMG signal may represent a less random and more orderly recruited firing pattern during the pedaling task at higher effort levels. **Key Words:** PEDALING, EMG, SAMPLE ENTROPY, MUSCLE, COORDINATION

Cycling has been widely studied by scientist as a repetitive activity requiring coordinated muscle recruitment to apply force to the pedals. Understanding the neuromuscular mechanisms of pedaling requires quantification of the timing and magnitude of lower limb muscle activation. It allows quantifying the function of individual muscles and their contribution to characteristic phases within the repeating movement cycle. This was first accomplished by Houtz and Fisher (15) and has been repeated by several independent laboratories (for a review, see [16,28]).

The musculoskeletal system has typically more muscles available than required to complete rhythmic movement tasks. This leads to a variety of solutions, which we refer to as solution space, to solve a specific task without changing the result (20). Owing to the musculoskeletal redundancy, the precise coordination between multiple muscles is an important characteristic in addition to the magnitude and timing of muscle activation, especially for high levels of power output (37). The timing of activation refers to the onset and offset when a muscle is active during a movement. Muscle coordination describes the contributions of individual muscles and/or muscle groups to the movement of interest (38) by analyzing the entire neuromuscular activation pattern instead of treating muscles as independent units. Zajac et al. (38) have proposed a model of muscle coordination with a synergistic behavior between knee and hip extensors as well as ankle plantar flexors. Whereas knee extensors are well suited to produce leg power, the ankle plantar flexors are coactivated to stiffen the ankle joint, keeping the foot stable to transfer the leg energy into a tangential pedal force for propulsion (38).

This coordinated behavior for force production is load dependent during pedaling, as lower limb joint power production increases in a joint-specific manner with increased mechanical demand (6). Such an altered challenge for the musculoskeletal system may affect muscle coordination patterns similarly as the relative power production for the task changes (6). In fact, it was shown previously that changes in power production are accompanied by changes in coactivation of muscle pairs (21). Extending this work to study muscle coordination of multiple muscles may prove useful to understand how the musculoskeletal system solves the same task with altered mechanical demands from a neuromuscular perspective.

A more conceptual rationale for studying muscle coordination is the proposal that muscles do not work as independent units. However, researchers have typically taken a reductionist approach with the analysis focused on the individual muscle. Although this approach has been successfully used in the past, it fails to provide a comprehensive

Address for correspondence: Hendrik Enders, B.Sc., Human Performance Laboratory, Faculty of Kinesiology, University of Calgary, 2500 University Drive NW, Calgary, Alberta, Canada, T2N 1N4; E-mail: henders@kin.ucalgary.ca.
Submitted for publication June 2014.
Accepted for publication October 2014.

0195-9131/15/4707-1450/0
MEDICINE & SCIENCE IN SPORTS & EXERCISE®

DOI: 10.1249/MSS.0000000000000564

analysis of the complexity of the neuromuscular strategy used by the musculoskeletal system during movement. Addressing the coordinative aspects of muscle activation may offer advantages to understand neuromuscular strategies without splitting it into individual anatomical units.

One tool that seems to be useful for studying muscle coordination is principal component analysis (PCA). This analysis method has been used in cycling to assess changes in muscle activity with fatigue (31) and different workloads (35). It was suggested that increasing the power output results not only from increased magnitude of muscle activation but also from changes in specific muscle coordination patterns (36). Principal component analysis can be used as an efficient tool to investigate if muscle specific contributions and temporal muscle coordination are adjusted in a load-dependant fashion similar to lower limb joint power production (6).

One aspect that has received little attention is the variability of muscle coordination and if this variability changes with different muscular demands. Whereas variability of waveforms (25) and of muscle coordination between cyclists (17) has been assessed previously, nobody has investigated the trial-to-trial variability of muscle coordination as well as the short-term fluctuations in the EMG signal of one pedal revolution. Analysis of variability in human movement is important, as it reflects and allows for the quantification of the neuromuscular control processes (12,13). Previously, we have shown a structured trial-to-trial amplitude variability of the EMG signal during cycling, which was interpreted as a neuromuscular adjustment to the altered environmental task constraints (7).

In addition to the amplitude variability, there are short-term fluctuations within the EMG power (envelope of the raw signal) during each pedal cycle that may provide valuable information. These fluctuations describe the adjustment of muscle activation within each pedal revolution. A random superposition of motor unit firing would result in random short-term fluctuations without organized structure. However, similar to the structure within the amplitude component of muscle activation strategies, an underlying structure may be present in the short-term temporal fluctuations of the EMG signal during cycling. If increased muscular demand leads to different motor unit firing rates, which is commonly the case (5), one may expect differences in the regularity of the short-term fluctuations in the EMG signal during cycling. Finding increased structure in the short-term fluctuations may be an indicator of neuromuscular control processes. In fact, it has been suggested previously that correlated firing of motor units may be a mechanism by which the central nervous system reduces the individual degrees of freedom to be controlled (8,27).

To the best of our knowledge, nobody has quantified the short-term fluctuations in the EMG signal during cycling. Ordered structure in these short-term fluctuations may indicate neuromuscular control and can be assessed using a newly developed method (40) based on sample entropy calculations (SampEn) (3,23). The obtained result, the entropic half-life (EnHL), was shown to be able to sensitively detect changes (1) and can be compared to a phase-randomized surrogate signal. Using a phase-randomized surrogate signal allows for the power spectrum of the measured signal to be unchanged while randomizing the structure encoded in the phase of the signal.

Therefore, the purpose of this study was twofold. The first purpose was to identify muscle activation strategies at different power outputs using PCA to quantify muscle coordination during cycling. The second purpose was to explore the identified strategies with respect to variability and regularity of the principal component (PC) scores reflecting the correlated muscle activation while pedaling. We hypothesized (H1) that muscle coordination will change with increased power output similar to the redistribution seen with joint power production (6) and changes in muscle coactivation (21). We further hypothesized (H2) that the regularity of the short-term fluctuations of the correlated muscle activation assessed with the EnHL increases with the increased mechanical demand. Based on the second hypothesis, we further proposed (H3) that the experimental EMG signal is characterized by a higher regularity compared to phase-randomized surrogate data for both load conditions.

Whereas the first hypothesis addresses our understanding of how humans adapt muscle coordination to achieve high-power output, the second two hypotheses deal with a novel way to extract neuromuscular control strategies from the surface EMG signal. Typically, frequent fluctuations in the EMG signal are treated as random, thus not providing any information. However, if our third hypothesis is confirmed, one may conclude that the fluctuations in the EMG are a result of a nonrandom neuromuscular control process in the human body. To the best of our knowledge, this would be the first measure of the regularity of neuromuscular control based on the surface EMG during dynamic tasks in humans.

METHODS

Experimental protocol. Fourteen healthy, active male participants (mean (SD), 27.7 (4.0) years, 77.1 (4.0) kg, and 181.1 (7.5) cm) were recruited. Participants had to be free from injury for at least 6 months before data collection. Participants were active-endurance-type athletes exercising at least three times a week at the point of data collection. Participants were not limited to cyclists but had also competitive experience in soccer, cross country skiing, and running, to capture a variety of endurance-type athletes. Each participant gave written informed consent in accordance with the University of Calgary's policy on research using human subjects and completed a Physical Activity Readiness Questionnaire. The study was approved by the University of Calgary Conjoint Health Research Ethics Board.

Electromyographic signals were recorded while subjects were pedaling on a calibrated velotron dynafit pro cycle ergometer (RacerMate Inc, Seattle, WA). The participants were comfortably seated on the ergometer, allowing a knee

flexion angle of approximately 5° at the bottom dead center. After a standardized 10-min warm-up, data were collected at 150- and 300-W power output in a randomized fashion while participants were pedaling at a frequency of 90 revolutions per minute (rpm). Participants were provided visual feedback of their cadence and instructed to keep it as close as possible to the target cadence of 90 rpm. Therefore, the difference between both experimental conditions is the force applied to the pedals by the lower limb muscles. Between both conditions, a 5-min rest period was allowed to avoid fatigue. The pedal position was determined using a magnetic switch that sent a square wave pulse when the right pedal crank passed 90° counterclockwise from the top dead center (TDC). For each condition, 60 s of data were recorded and the middle 70 pedal revolutions were used for further analysis.

EMG recordings. Surface EMG signals were recorded from seven leg muscles. Bipolar Ag/AgCl electrodes (10-mm diameter, 22-mm interelectrode distance) were placed after removal of the hair, abrasion with sandpaper, and cleaning with isopropyl wipes on the muscle bellies of the tibialis anterior (TA), soleus (SOL), gastrocnemius medialis (GM), biceps femoris long head (BF), vastus medialis (VM), rectus femoris (RF), and vastus lateralis (VL) on the right leg according to the recommendations of the Surface ElectroMyoGraphy for the Non-Invasive Assessment of Muscles guidelines (14). A ground electrode was placed on the tibial tuberosity; and all electrodes, cables, and amplifiers were taped to the skin to reduce movement artifacts. Electromyographic signals were amplified (Biovision, Wehrheim, Germany) with an amplification factor of 2500, band pass filtered (10–500 Hz) and recorded with a sampling frequency of 2400 Hz via a 12-bit A/D converter (National Instruments, Austin, TX).

EMG processing and PCA. For each of the seven muscles, the myoelectric signals were resolved into the power extracted by nine frequency bands (19–330 Hz) using a wavelet analysis (30). Individual trials corresponding to one full crank revolution were selected based on the signal from the magnetic pedal switch. For the PCA, each trial was time normalized to 720 samples corresponding to the 360° crank revolution. The total power summed across all frequency bands (EMG power) of the myoelectric signal was represented as a vector with seven components representing the EMG power of all seven muscles at each position in the pedaling cycle. These column vectors were appended forming a matrix of N = 705,600 (14 subjects × 70 pedal revolutions × 720 crank angles) EMG power vectors that span a seven-dimensional vector space. The EMG power for both conditions was normalized to the mean EMG power obtained for each muscle during the 150-W condition across all trials. For each condition, the mean of the vectors was subtracted from the matrix. Applying PCA to the input matrix results in a set of PC vectors and their corresponding eigenvalues of the matrix. The PC vectors were numbered ($PC_{\#}$-vector) in decreasing order of the eigenvalues. The eigenvalues represent the explained variance by each component number and is expressed as a percentage of the sum across all eigenvalues. Therefore, the first PC vector indicates which muscles contribute most strongly to the overall EMG pattern during the movement. The elements of the PC vectors are called the PC loadings. The projections of any EMG power vector on a PC vector are called a principal component (PC) indexed with the component number; they are often called PC weights or PC scores. Principal components were visualized as a function of pedal revolutions (720 crank angles) and formed a waveform for each component number. Coordination and trial-to-trial variability of muscle activation were visualized as trajectories in the plane spanned by the first two PCs.

Entropy calculation. Information theory defines entropy and sample entropy (SampEn) as the rate of information generation within a signal and quantifies the regularity in the signal (23). It can be conceived that points measured at short time intervals (small scales) may show nonrandom amplitude differences, and points measured at very large time intervals (large scales) are uncorrelated or represent random amplitude differences. Thus, with increasing time intervals between adjacent measured values (increasing scale), a transition from correlated to randomness between neighboring points occurs. A freely available software package (11) was used to calculate SampEn for each time series. A new reshape scale method was used to compute a reshape scale transition of SampEn (40). As an example, a reshape scale of three of the example time series of [1 2 3 4 5 6 7 8 9 10 11 12] will result in a new time series consisting of blocks [1 4 7 10 2 5 8 11 3 6 9 12]; in this example, the block size is four elements long. Thus, increasing the reshape scale will result in an increasingly larger time interval (Δt) between adjacent points in the reshaped time series (40). In this study, the reshaping procedure was expanded by randomizing the blocks within the reshaped time series, which represents a necessary addition to prevent the reordering of the elements, which occurs at large scales. For each individual signal, the SampEn was normalized to the maximum SampEn that was obtained by averaging the SampEn of four completely randomized signals. A reshape scale SampEn transition was obtained by computing the SampEn for gradually increasing scales. The EnHL was quantified as the scale at which the normalized SampEn equals 0.5.

Application of reshape scale SampEn transitions. The cycling movement induces an underlying basic repetitive temporal structure to the PCs seen in the waveforms that is caused by the pedaling rate. To analyze the structure of the short-term fluctuations in the EMG power, the PCs were filtered using a wavelet high-pass filter (3-dB cutoff frequency: 2.5 Hz) to remove the underlying base structure induced by the pedal revolution (90 rpm = 1.5 Hz).

Entropic half-life was used to assess the regularity in the high-pass–filtered PCs temporal structure. EnHL was computed for the 150- and 300-W conditions for each subject using the high-pass–filtered PCs(t) in absolute time units (not normalized to crank angle) of all 70 consecutive pedal revolutions.

Phase-randomized surrogate data. One surrogate signal was generated for the 150- and 300-W condition of

each subject for comparisons with the original, high-pass–filtered PCs. The original signal was Fourier transformed, then the phase was randomized, and a surrogate signal was obtained by applying an inverse Fourier transform. Thus, the surrogate signal has the same power spectrum and autocorrelation as the original signal; however, the structure encoded in the phase has disappeared.

Statistics. Analysis of variance (ANOVA) was used to assess statistical differences of the EnHL between the four conditions (150 W, 300 W, 150-W surrogate, 300-W surrogate). A factorial design was used when assessing differences in the EnHL for individual PCs. Inflation of type I error rate was avoided using a Bonferroni correction. A one-way ANOVA was used when comparing the overall EnHL between the four tested conditions. All tests were considered significant at $\alpha = 0.05$.

RESULTS

Principle component analysis. The result of submitting the EMG vectors (seven components each) to the PCA showed that the PC of the first six and four PC vectors were sufficient to explain more than 95% of the variance of the dataset for the 150- and 300-W pedaling conditions, respectively. This indicates a reduction of the dimensionality of the solution space for the 300-W condition that was required to explain 95% of the variance. In the 150-W condition, the first two PC vectors explained 30.9% and 26.7% of the total variance, respectively. The 300-W condition was strongly dominated by PC_1, which explained 71.3% of the total variance. This is roughly equal to the cumulative variance explained by the first three component numbers in the 150-W condition.

Visual inspection of the PC_1-vector loadings of the 150-W condition and the PC_2-vector of the 300-W condition showed largest loadings for BF, GM, and SOL (ankle and knee flexor muscles) (Figs. 1A, H). The loadings of the PC_2-vector of the 150-W condition and the PC_1-vector of the 300-W condition were largest for VM, RF, and VL (knee extensor muscles) (Figs. 1B, G). This demonstrates that the strategies (knee/ankle flexor and knee extensor) represented by the first two PC vectors are reversed for the 150- and 300-W condition (Fig. 1). This inversion was considered for the remainder of the analysis. Additionally, PC_2-vector of the 150-W condition is split into two different strategies in the 300-W condition. The first strategy is represented by the activation of the biarticular rectus femoris (PC_1-vector), and the second strategy groups the monoarticular VM and VL (PC_3-vector).

Although the loadings of PC_1-vector and PC_2-vector for both conditions grouped similar muscles, a difference can be observed in the distribution of the PC loadings between the two conditions. In the 150-W condition, three muscles (BF, GM, and SOL for PC_1-vector and VL, RF, and VM for PC_2-vector) show approximately equal loadings on the first two PC vectors. In the 300-W condition, the first two PC vectors are dominated by loadings of the RF and BF, respectively. Beyond the first two components, the PC loadings between the two conditions diverge. The PC_3-loadings in the 150-W condition are strongly dominated by the activation of the tibialis anterior, a muscle that plays almost no role in the 300-W condition, whereas the PC_3-loadings indicate a correlated activation of the VL, VM, and SOL in the 300-W condition. In the 150-W condition, all three knee extensor muscles are grouped in PC_2-vector, whereas a decoupling between the RF (PC_1-vector) and the VL and VM (PC_3-vector) can be observed in the 300-W condition (Fig. 1).

The PCs are visualized as waveforms (PCs for 720 crank angles) in Figure 2. The waveforms change in a similar way as the crank angle progresses in each of the pedal revolutions. The average waveforms across all pedal revolutions form an average waveform for each component number (Fig. 2). The second and first waveforms in the 150- and 300-W conditions, respectively, are similar, with a clear peak

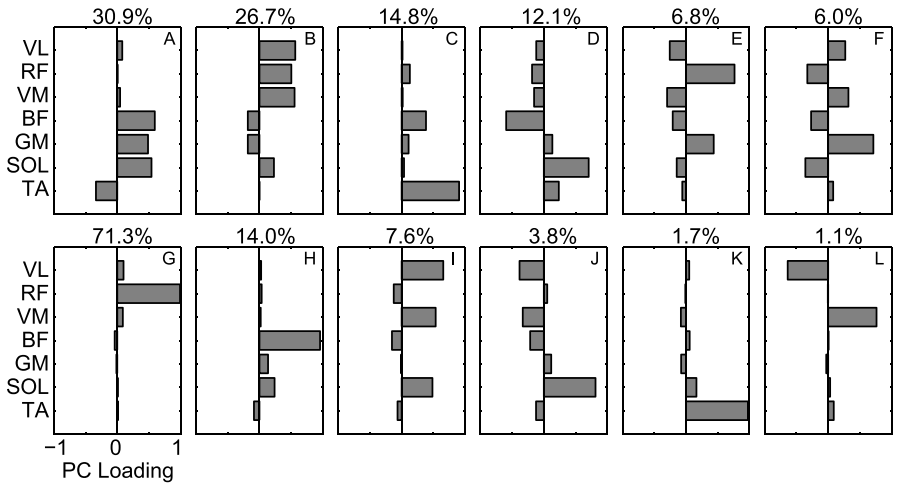

FIGURE 1—Principal component loadings (*horizontal axis*) of the seven muscles (*vertical axis*) on the first six PCs (from left to right) for the 150- (*top*) and 300-W (*bottom*) conditions. All *horizontal axes* have the same scaling as indicated by the *lower left* example. The number on *top of the boxes* indicates the explained variance in percent for each $PC_{\#}$-vector.

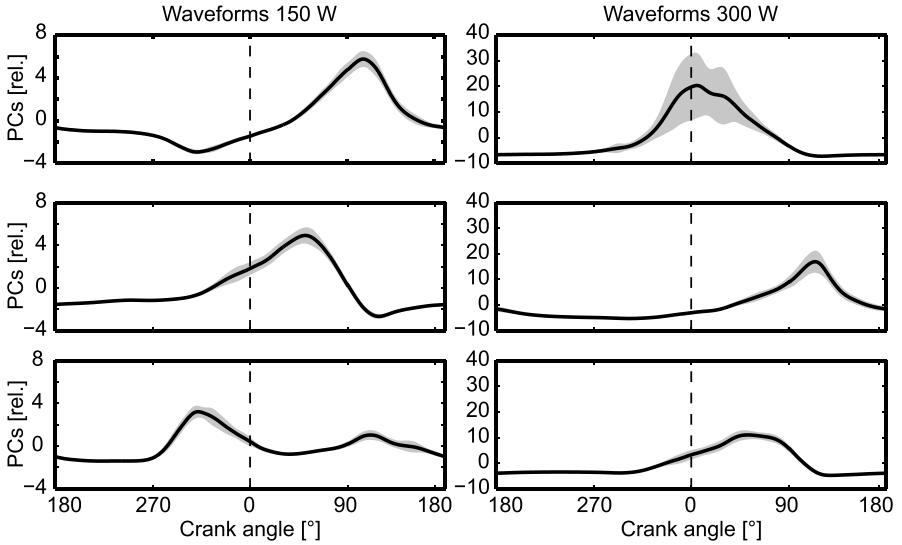

FIGURE 2—The first three average waveforms (*solid black line*) of 70 pedal revolutions for the 150-W condition (*left*) and 300-W condition (*right*). The *horizontal axis* describes the crank angle where the *dashed line* indicates when the crank passes the TDC. The *gray shaded area* represents the 95% confidence interval.

activity during the power production phase after the crank passes the TDC. The first and second components in the 150- and 300-W conditions, respectively, show a slightly later peak during the downstroke of the pedaling movement. The waveforms of the first two components are reversed for the 150- and 300-W conditions, thus confirming the reversal shown for the corresponding PC loadings.

Whereas the first waveform and the second waveform for the two conditions, respectively, are very similar, the explained variance corresponding to this waveform is much higher in the 300-W condition. In contrast to the first two waveforms, the higher-ordered waveforms showed no similarity. The third waveform can be seen in Figure 2 to illustrate the lack of similarity that was found for all higher waveforms.

Entropic half-life of the PCs. Visual inspection of the waveforms showed that there were short time fluctuations on top of the individual waveforms. The fluctuations reflect the variation of the activation of the muscles during the cycles of the pedal revolutions. The high-pass–filtered PCs(t) that reflect these fluctuations over time showed a distinct transition from an ordered, correlated relation between consecutive time points to a random relationship between neighboring points when computing the SampEn for different scales (Fig. 3).

The EnHL of this transition was computed for each of the PC(t) for the 150 W, the 300 W, and their surrogates (Fig. 4). A significant main effect of the EnHL of all PC vectors was found when comparing all four tested conditions ($F_{1,13}$ = 2856.4; $P < 0.001$). Significant differences in the EnHL for the 150 W, the 300 W, and their surrogates were consistently found for each individual component number (Fig. 4). All individual PCs showed a significantly longer EnHL in the 300-W experimental condition compared to the 150-W

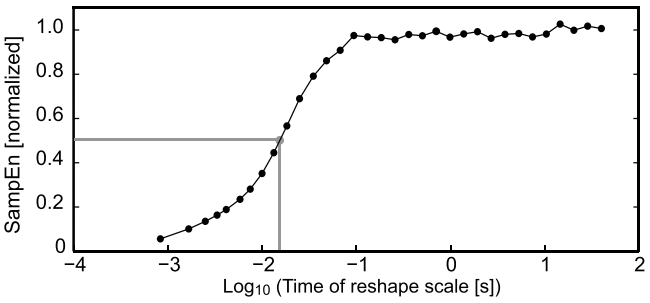

FIGURE 3—Transition curve of SampEn for different reshape scales ranging from Δt 1.7 ms to 40 s. The entropic EnHL is the reshape scale for which the normalized sample entropy is 0.5 (*gray dot*). Reshape scales on the horizontal axis are shown as a log plot for better visualization.

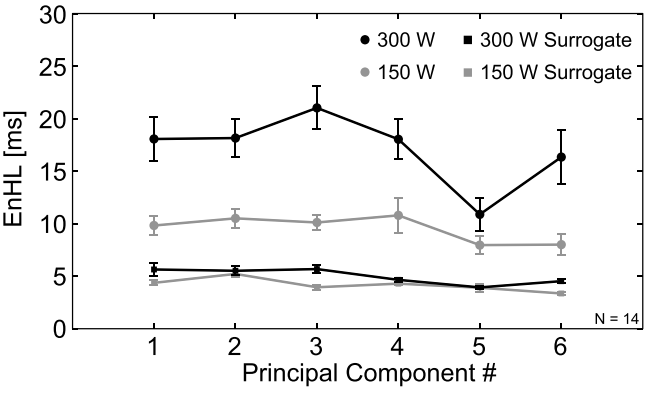

FIGURE 4—The EnHL for temporal PC fluctuation corresponding to individual component numbers for the 150- and 300-W experimental conditions (*circles*) as well as their corresponding surrogate conditions (*squares*). The *lines* of the 150- and 300-W conditions are shown in *gray* and *black*, respectively. Each data point represents the mean across subjects (N = 14), with the *error bars* indicating the 95% confidence interval.

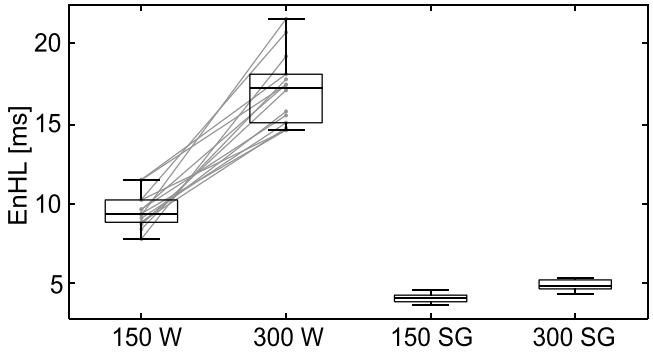

FIGURE 5—*Boxplots* for the EnHL for the 150- and 300-W experimental conditions and both corresponding surrogate conditions. The lines connect the EnHL for each individual in both experimental conditions. Note that all 14 participants show an increase in the 300-W condition. Both surrogate conditions are significantly lower compared to both the 150- and 300-W experimental conditions.

experimental condition ($P < 0.001$). Both the 150- and 300-W experimental conditions showed significantly longer EnHL compared to each surrogate condition ($P < 0.001$). However, there was a significant difference ($P < 0.001$) in the EnHL of the respective surrogate data for PC_1, PC_3, and PC_6; whereas PC_2, PC_4, and PC_5 did not show statistically significant differences ($P > 0.05$).

The ANOVA of the overall EnHL (EnHL averaged across all PC weights of the 95% solution space) showed a significant main effect of the tested conditions ($F_{1,13} = 2582.72$; $P < 0.001$). Post hoc comparisons showed that across all 14 subjects, the overall EnHL was significantly longer in the 300-W condition compared to the 150-W ($P < 0.001$). In detail, the transition from being more regular to more random with increasing scale occurred at EnHL = 16 ms in the 300-W condition and at EnHL = 9 ms in the 150-W condition (Fig. 5). This represents an increase in the EnHL of 68.4% as power output doubled.

The overall EnHL for the 150-W and 300-W surrogate data were 4.1 and 4.7 ms, respectively. However, the mean EnHL of the surrogates, although they are not very different in absolute terms, are significantly different ($P < 0.01$). Both the 150- and 300-W experimental conditions had a significantly longer EnHL compared to the 150-W and 300-W surrogate data ($P < 0.001$).

Muscle coordination. Muscle coordination was visualized as trajectories of the PCs in the plane spanned by the first two PC vectors of each condition (Fig. 6). This plane represents the two dominant coordinated recruitment patterns while performing the cycling task in each condition. The zero crossover point represents the mean muscle activity. As mentioned previously, the first two component numbers were reversed in the 300-W condition compared to the 150-W condition. It can be seen that the general activation pattern, represented by the loop trajectories, is similar in both conditions, although there seem to be major differences in magnitude and variability of these trajectories.

In the 150-W condition, the initial activation as the crank passes the TDC is a coordinated activation of knee extensor (PC_1) and knee flexor and ankle flexor (PC_2) muscles indicated by an angled positive slope (light blue to yellow). Contrary to this behavior, the 300-W condition is initially characterized by an almost vertical slope (light blue to green) indicating a dominant muscle activation of the knee extensors (PC_1), primarily the RF muscle. After the upper turning point in Figure 6 (green to yellow) in the 300-W condition,

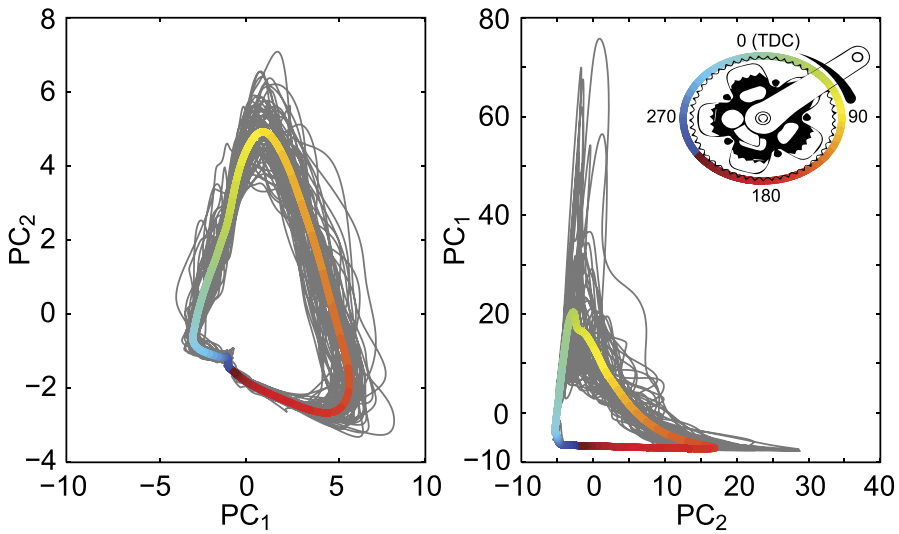

FIGURE 6—Coordination plots visualized as loop trajectories in the solution space spanned by the first two principle components for 150 W (*left*) and 300 W (*right*). The color code represents the crank angle at each time point and is visualized in the *top right corner*. The first and second PCs in the 150-W condition represent the BF, GM, and SOL and the VL, VM, and RF, respectively. For the 300-W condition, the first and second PCs show activity of the RF and BF, respectively. Whereas the other muscles also contribute to the first two components in the 300-W condition (see Fig. 1), their relative contributions are negligible compared to the magnitudes of RF and BF.

the PCs show a negative slope (yellow to orange), indicating a coordinated relaxation of the knee extensor and simultaneous activation of the knee flexor muscles. As the knee extensors are fully relaxed, the knee flexors develop their full activation around 120° past the TDC (orange). A similar pattern is seen in the 150-W condition during the transition from 90° (yellow/orange) to 180° (red). In the 300-W condition, the knee flexor muscles relax, whereas activity of the knee extensor muscles is unaffected until slightly before the crank passes the TDC. This results in an almost horizontal line (red to purple) for the 300-W condition in Figure 6, indicating again a dominant pattern of the knee flexors (PC_2) with the knee extensors being relaxed. In contrast, during the 150-W condition, the last half of the crank revolution (red to light blue) is characterized by a slope indicating an activation of the knee extensor muscles (PC_2) during the relaxation phase of the knee flexor and ankle flexor muscles (PC_1).

DISCUSSION

This study investigated muscle activity during cycling using a PCA approach that has previously been used for the analysis of gait kinematics (4,10,18,32). Similar to these studies, we were able to identify main activation patterns reflected in the EMG power, thus showing the coordination of muscle activity while cycling. The muscle coordination in this study was visible in the loadings of the PC vectors (Fig. 1). This approach expanded on studies that reported the onset and end of muscle activity and global waveforms of muscle activity while cycling (2,25).

The results of this study showed that specific muscle activation profiles (e.g., RF) take over a more dominant role as power output increases and that the knee extensors and ankle plantar flexors had more distinctly separated times of activation at higher effort levels. Increasing the power output was also characterized by a reduction in the solution space as seen by the lower number of PC vectors necessary to capture 95% of the variance of the data in the high-power condition. We suggest that this result is primarily due to the increased mechanical task constraints that decrease the number of options for the musculoskeletal system to solve the pedaling task. This result confirms a basic physical principle that completing a task in an unspecified manner allows for a theoretically infinite number of solutions. However, an increase in task constraints (e.g., completing a task as fast as possible, approaching maximum-power output) results in a decreased number of available solutions for the system to complete the task successfully (20). Previous studies on pedaling support this reduction in the solution space as the task becomes more constrained when considering the magnitude characteristics of an EMG signal (7).

Muscle function during pedaling. The reduced solution space in the 300-W condition was strongly characterized by an activation of knee extensors (RF), knee flexors (BF), and ankle plantar flexors (SOL); however, the knee muscles played a dominant role. It was previously shown that lower limb joint power production increases substantially as mechanical power production increases (6), with the knee extensor and flexor muscles providing more relative joint power compared to the ankle muscles (6) and the RF muscle activation being strongly associated to the produced power output (21). In fact, it was shown that muscular efficiency increases with higher levels of power output at a given cadence (39). This suggests that the observed changes in neuromuscular strategy during the 300-W condition may be one of the mechanisms of how efficiency is optimized. In support of this argument, Rouffet et al. (24) reported changes in EMG activity and timing of the RF and BF muscles (PC_1 and PC_2 in the 300-W condition) when subjects pedaled at a low-power output (i.e., unloaded cycling exercise). This change in neuromuscular strategy was associated with increased oxygen consumption (24). Combining the results in this study and previously reported findings suggests that power-induced changes in the neuromuscular strategies during cycling seem to involve the RF and BF muscles leading to different outcomes depending on the power produced by the individual.

The coordination between muscles in the high-power output condition also confirms a mechanical model that was proposed for the pedaling movement (38), where the knee and hip extensors contract during leg extension to produce substantial leg power. However, the knee and hip extensors do not deliver much of this energy to the crank. Instead, the plantar flexor muscles that produce little leg power are active to redistribute the power by reducing leg energy and concurrently increasing energy delivered to the pedal to produce a tangential pedal force (38). This synergistic behavior of the hip and knee extensors and the ankle plantar flexors permits the foot to remain nearly horizontal, allowing efficient energy redistribution from the leg to the crank (38). This mechanical synergistic behavior was confirmed based on the EMG results of this study.

The 300-W condition showed a main pattern that was very close to the EMG profile of the RF. This biarticular muscle acts as a hip flexor and knee extensor and is crucial for power production during the propulsion phase and also for power transfer between the hip and the knee joint (25). This suggests that energy redistribution between the hip and the knee joint seems to be an important characteristic in the muscle activation strategy during high-power output. In fact, it was proposed that power produced by monoarticular muscles is transferred to adjacent joints by their biarticular antagonists (29). Others have suggested a unique role for biarticular muscles due to their capability of redistributing energy among different body segments rather than transferring power between joints (38). A common core to these concepts is the unique role of acting on multiple joints and segments and thereby offering solutions different from a single or even multiple monoarticular muscles. This suggests that the RF muscle plays a key role for segment coordination between pelvis and thigh and redistributing the energy produced by knee and hip muscles.

PCA reveals coordination strategies. Similar to the studies done on kinematics (4,10), the PC loadings provided a holistic picture on the correlated activation of different muscles and the proportional contribution of individual muscles to the overall EMG activity. In the 150-W condition, we observed that ankle and knee flexors were grouped into PC_1-vector, indicating a correlated firing of the BF, GM, and SOL. Similarly, the three quadriceps muscles were grouped into PC_2-vector, indicating a correlated firing of all three muscles. Both PC vectors contributed almost equally to the overall muscle activation strategy, indicating a balanced role from the knee and ankle muscles. The 300-W condition was characterized by two systematic changes in the loadings of the first two PC vectors. First, the loadings on PC_1-vector and PC_2-vector were clearly dominated by the RF and BF, respectively, thereby reducing the role of the ankle flexors. Second, the proportional contribution of PC_1-vector was approximately five times higher than PC_2-vector in the 300-W condition, indicating a clear dominance of the knee extensor muscles over the knee flexor muscles. In summary, the changes from 150 W to 300 W can be described as a proportional increase in knee muscle activation compared to the ankle activation. With higher mechanical demand, knee muscle activation increases substantially for leg power production, whereas the demand for a stiff ankle joint necessary for efficient energy transfer to the crank is similarly relevant in the 150- and 300-W conditions. Lastly, the activation of the biarticular RF and both monoarticular VL and VM were decoupled in the 300-W condition, indicating different roles during the movement cycle. This uncoupling supports the idea for different roles of biarticular and monoarticular muscles during cycling (29,38).

Variability of the neuromuscular strategy. Previous studies have shown structured components in the amplitude trial-to-trial fluctuations (7), indicating a nonrandom control that may be involved during pedaling. However, only the amplitude fluctuations were considered in the analysis neglecting the information encoded in the phase. It is known that the phase of the signal contains information (22), which gave rationale to the analysis of the EMG signal in this study to quantify the short-term fluctuations within a pedal revolution using SampEn.

These short-term fluctuations in the overall EMG power of one pedal revolution may be caused by muscle activity that is responsible for the fine tuning of the movement. To quantify numerically the properties of EMG power fluctuations, we hypothesized that a new variable, the EnHL, which is based on the reshape scale transition of SampEn (40), would be able to reveal that the short-term fluctuations of EMG power were nonrandom but had a structure. In our case, structure may be interpreted as signal regularity where EMG power might be more consistently regulated by descending motor commands and/or other sensory inputs or reflexes. The first major result of the SampEn analysis showed that there was a significant increase in the EnHL for all subjects and components, indicating a greater amount of structure in the EMG power encoded in the phase of the signal. Second, this study proved that a large amount of the regularity is encoded in the phase of the EMG power and changes with the power output during cycling. The combination of these two results leads to two main interpretations. First, we conclude that structure in the signal increases with task difficulty most likely due to a more constrained solution space that allows for less randomness in the execution of a movement task. Second, the structure encoded in the phase of the short-term fluctuations of the EMG power might indicate neuromuscular control mechanisms within the human body. This is based on the observation that randomizing the phase while keeping all other aspects of the signal unaltered, particularly the autocorrelation, resulted in a substantial drop of the EnHL. It shows that the observed structure in the EMG power is significantly different from an uncontrolled random process.

Entropy has been widely used as an analysis tool to assess physiological signals such as the electrocardiogram (3,23). SampleEn has not yet been used in the context of EMG signals during rhythmic locomotion. Electromyographic signals are a superposition of motor unit action potentials from numerous motor units in the muscle. A random firing of motor units located under the electrode will result in a random EMG signal with no underlying structure and no regularity in the short-term fluctuations of the EMG power. It was previously shown that single motor unit discharge variability continuously decreases with increasing force output (33). As a result of increased motor unit discharge regularity, the overall EMG signal and, thus, the short-term fluctuations within the signal, may become more regular. Our results suggest that motor unit firing during both low- and high-power output cycling is nonrandom in support of previous comparisons of the time-dependent EMG structure to surrogate data during isometric force production (34). The further increase in regularity in the 300-W condition suggests increased neuromuscular control that may be a result of increased synchrony in the firing of the motor units. However, the recordings in this experiment were superficial and do not allow measurement of specific motor unit populations. Therefore, the translation of muscle tissue under the electrode, which might be different in the two experimental conditions owing to muscle gearing and fascicle mechanics, should be considered as a limitation of surface EMG recordings in this study.

It is well described that increased motor unit synchronization is an important factor for muscle activation and force development (26). It is further argued that a great benefit of motor unit synchronization is the coordination of multiple muscles (26) resulting in skilled muscle synergies. We might speculate that our increased regularity is based on this altered motor unit firing to improve muscle coordination for increased force development. Some studies speculate that increased motor unit synchronization may be a result of an enhanced descending drive from cortical areas (19). If motor unit synchronization is dependent on a functional

descending corticospinal pathway, which is supported by studies using neurologically impaired subjects (9), then it might be speculated that the descending drive to the motor units and muscles is enhanced in the 300-W condition compared to the 150-W condition. However, this speculation needs careful evaluation using measurements that combine electrophysiological signals of muscles and cortical areas.

CONCLUSIONS

This study evaluated intertrial and intratrial variability of myoelectric signals during pedaling at different power outputs. Overall, the result suggests that the solution space becomes more defined as task-difficulty increases, which leads to a more regular signal with respect to the short-term fluctuations. Additionally, alterations in muscle activation strategy were apparent, as there was a redistribution of the importance of muscles contributing to the movement.

Conflicts of Interest and Source of Funding: There are no professional relationships with companies or manufacturers to disclose for all authors.

This research was supported by the Natural Sciences and Engineering Research Council of Canada, the da Vinci Foundation, and the Biomechanigg Research Inc. The results of the present study do not constitute endorsement by the American College of Sports Medicine.

REFERENCES

1. Baltich J, von Tscharner V, Zandiyeh P, Nigg BM. Quantification and reliability of center of pressure movement during balance tasks of varying difficulty. *Gait Posture*. 2014;40(2):327–32.
2. Baum BS, Li L. Lower extremity muscle activities during cycling are influenced by load and frequency. *J Electromyogr Kinesiol*. 2003;13(2):181–90.
3. Costa M, Goldberger AL, Peng C-K. Multiscale entropy analysis of complex physiologic time series. *Phys Rev Lett*. 2002;89(6):068102.
4. Daffertshofer A, Lamoth CJC, Meijer OG, Beek PJ. PCA in studying coordination and variability: a tutorial. *Clin Biomech (Bristol, Avon)*. 2004;19(4):415–28.
5. De Luca CJ, Roy AM, Erim Z. Synchronization of motor-unit firings in several human muscles. *J Neurophysiol*. 1993;70(5):2010–23.
6. Elmer SJ, Barratt PR, Korff T, Martin JC. Joint-specific power production during submaximal and maximal cycling. *Med Sci Sports Exerc*. 2011;43(10):1940–7.
7. Enders H, Maurer C, Baltich J, Nigg BM. Task-oriented control of muscle coordination during cycling. *Med Sci Sports Exerc*. 2013; 45(12):2298–305.
8. Farmer S. Rhythmicity, synchronization and binding in human and primate motor systems. *J Physiol*. 1998;509(Pt 1):3–14.
9. Farmer S, Swash M, Ingram D, Stephens J. Changes in motor unit synchronization following central nervous lesions in man. *J Physiol*. 1993:83–105.
10. Federolf P, Tecante K, Nigg B. A holistic approach to study the temporal variability in gait. *J Biomech*. 2012;45(7):1127–32.
11. Goldberger AL, Amaral LAN, Glass L, et al. PhysioBank, PhysioToolkit, and PhysioNet: components of a new research resource for complex physiologic signals. *Circulation*. 2000;101(23):e215–20.
12. Harris C, Wolpert D. Signal-dependent noise determines motor planning. *Nature*. 1998;394:780–4.
13. Hausdorff JM, Zemany L, Peng C-K, Goldberger AL. Maturation of gait dynamics: stride-to-stride variability and its temporal organization in children. *J Appl Physiol*. 1999;86(3):1040–7.
14. Hermens HJ, Freriks B, Disselhorst-Klug C, Rau G. Development of rsecommendations for SEMG sensors and sensor placement procedures. *J Electromyogr Kinesiol*. 2000;10(5):361–74.
15. Houtz SJ, Fischer FJ. An analysis of muscle action and joint excursion during exercise on a stationary bicycle. *J Bone Joint Surg Am*. 1959;41-A(1):123–31.
16. Hug F, Dorel S. Electromyographic analysis of pedaling: a review. *J Electromyogr Kinesiol*. 2009;19(2):182–98.
17. Hug F, Turpin Na, Guével A, Dorel S. Is interindividual variability of EMG patterns in trained cyclists related to different muscle synergies? *J Appl Physiol*. 2010;108(6):1727–36.
18. Maurer C, von Tscharner V, Samsom M, Baltich J, Nigg BM. Extraction of basic movement from whole-body movement, based on gait variability. *Physiol Rep*. 2013;1(3):e00049.
19. Milner-Brown HS, Stein RB, Lee RG. Synchronization of human motor units: possible roles of exercise and supraspinal reflexes. *Electroencephalogr Clin Neurophysiol*. 1975;38(3):245–54.
20. Mueller H, Sternad D. Motor learning: changes in the structure of variability in a redundant task. *Adv Exp Med Biol*. 2009;629:439–56.
21. O'Bryan SJ, Brown N a T, Billaut F, Rouffet DM. Changes in muscle coordination and power output during sprint cycling. *Neurosci Lett*. 2014;576:11–6.
22. Oppenheim AV, Lim JS. The importance of phase in signals. *Proc IEEE*. 1981;69(5):529–41.
23. Richman J, Moorman J. Physiological time-series analysis using approximate entropy and sample entropy. *Am J Physiol Heart Circ Physiol*. 2000;278:H2039–49.
24. Rouffet DM, Mornieux G, Zameziati K, Belli A, Hautier CA. Timing of muscle activation of the lower limbs can be modulated to maintain a constant pedaling cadence. *J Electromyogr Kinesiol*. 2009;19(6):1100–7.
25. Ryan MM, Gregor RJ. EMG profiles of lower extremity muscles during cycling at constant workload and cadence. *J Electromyogr Kinesiol*. 1992;2(2):69–80.
26. Semmler JG. Motor unit synchronization and neuromuscular performance. *Exerc Sport Sci Rev*. 2002;30(1):8–14.
27. Semmler JG, Sale MV, Meyer FG, Nordstrom MA. Motor-unit coherence and its relation with synchrony are influenced by training. *J Neurophysiol*. 2004;92(6):3320–31.
28. So RCH, Ng JK-F, Ng GYF. Muscle recruitment pattern in cycling: a review. *Phys Ther Sport*. 2005;6(2):89–96.
29. Van Ingen Schenau GJ. From rotation to translation: constraints on multi-joint movements and the unique action of bi-articular muscles. *Hum Mov Sci*. 1989;8(4):301–37.
30. Von Tscharner V. Intensity analysis in time-frequency space of surface myoelectric signals by wavelets of specified resolution. *J Electromyogr Kinesiol*. 2000;10(6):433–45.
31. Von Tscharner V. Time-frequency and principal-component methods for the analysis of EMGs recorded during a mildly fatiguing exercise on a cycle ergometer. *J Electromyogr Kinesiol*. 2002;12(6):479–92.
32. Von Tscharner V, Enders H, Maurer C. Subspace identification and classification of healthy human gait. *PLoS One*. 2013;8(7): e65063 doi:10.1371/journal.pone.0065063.
33. Vaillancourt DE, Larsson L, Newell KM. Effects of aging on force variability, single motor unit discharge patterns, and the structure

of 10, 20, and 40 Hz EMG activity. *Neurobiol Aging*. 2003; 24(1):25–35.
34. Vaillancourt DE, Larsson L, Newell KM. Time-dependent structure in the discharge rate of human motor units. *Clin Neurophysiol*. 2002; 113(8):1325–38.
35. Wakeling J, Horn T. Neuromechanics of muscle synergies during cycling. *J Neurophysiol*. 2009;101(2):843–54.
36. Wakeling JM, Blake OM, Chan HK. Muscle coordination is key to the power output and mechanical efficiency of limb movements. *J Exp Biol*. 2010;213(3):487–92.
37. Wakeling JM, Blake OM, Wong I, Rana M, Lee SSM. Movement mechanics as a determinate of muscle structure, recruitment and coordination. *Philos Trans R Soc Lond B Biol Sci*. 2011;366(1570): 1554–64.
38. Zajac FE, Neptune RR, Kautz SA. Biomechanics and muscle coordination of human walking; Part I: Introduction to concepts, power transfer, dynamics and simulations. *Gait Posture*. 2002; 16(3):215–32.
39. Zameziati K, Mornieux G, Rouffet D, Belli A. Relationship between the increase of effectiveness indexes and the increase of muscular efficiency with cycling power. *Eur J Appl Physiol*. 2006;96(3):274–81.
40. Zandiyeh P, von Tscharner V. Reshape scale method: a novel multi scale entropic analysis approach. *Phys A Stat Mech Appl*. 2013; 392(24):6265–72.